Journal of Alloys and Compounds 819 (2020) 153361

Contents lists available at ScienceDirect

Journal of Alloys and Compounds

journal homepage: http://www.elsevier.com/locate/jalcom

AC electrical resonances in nanocomposites with partly oxidized FeCoZr grains embedded in CaF_2 ceramic matrix – effects of annealing

T.N. Kołtunowicz [a, *], V. Bondariev [a], P. Żukowski [a], J.A. Fedotova [b], A.K. Fedotov [b]

[a] Department of Electrical Devices and High Voltage Technology, Lublin University of Technology, 38a Nadbystrzycka St, 20-618, Lublin, Poland
[b] The Institute for Nuclear Problems of Belarusian State University, 11 Bobrujskaya St, 220006, Minsk, Belarus

ARTICLE INFO

Article history:
Received 13 August 2019
Received in revised form
8 December 2019
Accepted 9 December 2019
Available online 12 December 2019

Keywords:
Granular nanocomposites
Ceramic matrix
Oxidation
Annealing
Electrical properties

ABSTRACT

This paper presents the frequency and temperature dependences of the phase shift angle, the active part of the admittance, the capacitance, and the dielectric loss factor tanδ for as-deposited and annealed $(FeCoZr)_x(CaF_2)_{(100-x)}$ nanocomposite films prepared via ion-beam sputtering of a complicated target in a mixed argon–oxygen gas atmosphere. For films with a metallic phase content of $x = 62.7$ at.%, after 15 min of annealing at a temperature of 398 K, a strong 'negative capacitance' effect occurred, indicating an inductive-like contribution to the admittance. This effect was accompanied by two types of resonances: a voltage resonance and two current resonances. It was determined that description of AC parameters of $(FeCoZr)_x(CaF_2)_{(100-x)}$ films can be made by using compound equivalent circuit, consisting of RLC series circuit and two conventional circuits differing in values of their RLC elements, which means that the material can be used in microelectronics instead of such circuits.

The joint analysis of the $\sigma(f)$, $\theta(f)$, $C_p(f)$, and $\tan\delta(f)$ curves allowed the resonances to be explained on the basis of the previously developed alternating current (AC)/direct current (DC) hopping model with three different characteristic times of electron hopping.

1. Introduction

Nanocomposites, owing to the nanometric effects occurring in them, have found practical applications in many fields. Because of their large surface area-to-volume ratio, they are used in catalysts, solar cells, and gas sensors [1,2]. The change of the bandgap width in dielectrics and semiconductors with the reduction of the characteristic sizes allows the use of nanocomposites in optoelectronics [3]. Increasing the hardness and abrasion resistance improves the mechanical properties [4–6]. Many metal–dielectric nanocomposites show very promising magnetic [7–10] and AC/DC electrical [11–15] properties. In a low frequency range the admittance of $(CoFeZr)_x(Al_2O_3)_{(100-x)}$ and $(CoFeZr)_x(Pb(ZrTi)O_3)_{(100-x)}$ nanocomposite films is almost independent of the frequency at $f < 10$ kHz [16]. At higher f values, the admittance is saturated with frequency and reaches a nearly constant value. This property appears often in nanocomposite materials produced via ion-beam sputtering in a mixed argon–oxygen atmosphere. Annealing at high temperatures strongly changes the frequency dependence of the admittance and shifts the percolation threshold to higher values of x. Such behavior might be associated with the oxidation of the surface of metallic nanoparticles during the interaction of oxygen ions in the atmosphere of the vacuum chamber or during the following annealing procedure.

The mechanism of such specific behaviour of AC transport in $(CoFeZr)_x(Al_2O_3)_{(100-x)}$ and $(CoFeZr)_x(Pb(ZrTi)O_3)_{(100-x)}$ nanocomposite films was explained in our previous works [7,14,17,18]. According to these studies, the oxide 'shells,' which are formed around metallic 'cores' of nanoparticles either directly at deposition [19] or after the following high-temperature annealing [17], prevent their direct electric contact even beyond the electric percolation threshold [7,11]. As a result, the frequency dependences of the phase shift angle θ showed a very specific characteristic for the films with x around the percolation threshold. This resulted in a 'negative capacitance' effect (prevalence of the inductive contribution to the imaginary part of the admittance over the capacitive), which is usually observed at high frequencies and low temperatures in as-deposited samples [18–23]. In electrical engineering, such behavior is characteristic for *RLC* series equivalent circuits. The phase shift was $90° \leq \theta < 0°$ at low frequencies and $0° < \theta \leq 90°$ at

* Corresponding author.
E-mail addresses: t.koltunowicz@pollub.pl, tomasz.koltunowicz@gmail.com (T.N. Kołtunowicz).

https://doi.org/10.1016/j.jallcom.2019.153361

higher frequencies. Our measurements also show that for some frequency f_0, when the phase angle crosses the zero line ($\theta = 0^\circ$), the capacity modulo C_p of the nanocomposite film reaches its local minimum. This indicates the presence of a voltage resonance in the sample at f_0. Additionally, there is compensation of opposite phase voltages which are dropped on capacitive and inductive contributions of the impedance reactive parts of, which resulted in, occurrence of minimum on the frequency dependence C_p, as previously reported [17,19].

The occurrence of inductive-like properties in nanocomposite films is usually considered as evidence of the formation of oxide 'shells' around metallic nanoparticles during either deposition or annealing. We associate such behavior with the three-component structure of the studied nanocomposite films: *1* – metallic α-FeCo(Zr) 'core'; *2* – FeCo-based metallic oxide 'shell' around the metallic particle; *3* – dielectric matrix (Al_2O_3, $Pb(ZrTi)O_3$) [7,24,25]. The observed phenomenon of the inductive contribution domination in the admittance of non-coil-like nanocomposite structures was explained in Ref. [18] with a model of AC/DC electron hopping and experimentally verified in Refs. [11,18,19].

As shown in Refs. [7,11,16,18,19,24,25], the state of the 'shells' around the metallic 'core' (i.e., the phase composition of 'shell' oxides and their contribution relative to the metallic phase) is strongly dependent on the chemical composition of the matrix and the metallic element concentration x in the nanocomposite. Among inorganic substances, oxygen-containing dielectric compounds (such as alumina, $Pb(ZrTi)O_3$, and silica) are most commonly used as matrices. For example, a comparison of $(Fe_{45}Co_{45}Zr_{10})_x(Al_2O_3)_{(100-x)}$ and $(Fe_{45}Co_{45}Zr_{10})_x(Pb(ZrTi)O_3)_{(100-x)}$ samples sputtered in an oxygen-containing atmosphere revealed a significant difference in the structure of the nanoparticles inside the matrices. In the $(Fe_{45}Co_{45}Zr_{10})_x(Al_2O_3)_{(100-x)}$ nanocomposite films, the crystalline state of the metallic α-FeCo(Zr) 'core' inside the resistive oxidation amorphous alumina matrix remained above the percolation threshold, although the portion of FeCo-based 'shell' oxides increased with x [16,19,24,25]. $Fe_{45}Co_{45}Zr_{10}$ nanoparticles in the more chemically active lead zirconium titanium (PZT) matrix are fully oxidized during the deposition process, even at small x values [7,18].

The matrix in nanocomposite films is crucial for the formation of the 'core–shell' structure of metallic nanoparticles and hence their electrical properties. Additionally, surface oxidation of nanoparticles presumably depends on the intrinsic oxygen in the Al_2O_3 and $Pb(ZrTi)O_3$ matrices of the nanocomposite films, especially under heat treatment.

Thus, the aim of the present study was to investigate the effects of oxygen in the sputtering and annealing gas atmospheres on the temperature and frequency dependences of the AC conductance of nanocomposites containing CoFeZr nanoparticles embedded into an oxygen-free transparent ceramic matrix (CaF_2), in comparison with the previously studied $(Fe_{45}Co_{45}Zr_{10})_x(Al_2O_3)_{(100-x)}$ [19] and $(Fe_{45}Co_{45}Zr_{10})_x(Pb(ZrTi)O_3)_{(100-x)}$ [26] composite nanogranular films. Further task is to develop equivalent circuit describing the occurrence of resonance phenomena in the tested nanocomposites and analysis of the possibilities of their use for the production of elements with resonant circuit properties.

2. Experimental

We examined the electrical properties of $(CoFeZr)_x(CaF_2)_{(100-x)}$ nanocomposites by applying an AC. The nanocomposites were prepared via high-energy ion-beam sputtering of a compound target in a mixed argon–oxygen atmosphere in a vacuum chamber. The compound target contained a ferromagnetic alloy $Co_{45}Fe_{45}Zr_{10}$ plate covered with stripes of dielectric transparent ceramic CaF_2 through changing distances [27,28]. The pressures of argon and oxygen gas in the vacuum chamber were $p_{Ar} = 8.5 \times 10^{-2}$ Pa and $p_{O2} = 4.3 \times 10^{-3}$ Pa, respectively.

The chemical composition and nanogranular structure of the $(CoFeZr)_x(CaF_2)_{(100-x)}$ films were verified using X-ray microanalysis and transmission electron microscopy [11]. The obtained images indicate that practically spherical crystalline nanoparticles of a metallic phase covered with FeCo-based 'shells' were separated by the crystalline transparent ceramic matrix CaF_2. The average diameter of the nanoparticles was approximately 4.4 nm, with a standard deviation of approximately 0.22 nm.

For measurements of the frequency/temperature dependences of the real part of the admittance $\sigma(f, T_p)$, the phase shift angle $\theta(f, T_p)$, the capacitance $C_p(f, T_p)$, and the dielectric loss factor $\tan\delta(f, T_p)$, AC bridges HIOKI 3532 LCR HiTESTER (in the frequency range of 42 Hz–5 MHz) with a special personal computer-based control system were used. The electrical properties of the samples were measured after deposition and after the samples were subjected to isochronous (15 min) annealing in a tubular furnace in the temperature range of 398–573 K with steps of 25 K. The electrical parameters of the samples were measured in the temperature range of 77–373 K with steps of 5 K and an accuracy better than 1%. The measurement stand was described in Refs. [29,30].

3. Results and discussion

In our previous studies [11,31,32], we examined the structural, electrical (AC/DC), and magnetic properties of as-deposited $(FeCoZr)_x(CaF_2)_{(100-x)}$ nanocomposite films with $20 < x < 72$ at.%. In the present study, we examined in further detail the sample with $x = 62.7$ at.%, which exhibited specific electrical properties in the AC regime.

The measurement results for the as-deposited sample are presented in Fig. 1. Let us discuss the most characteristic features of these curves. As shown in Fig. 1a, the real part of the admittance increased slightly with the increase of the frequency at a relatively weak temperature dependence of $\sigma(T_p)$. Thus, for the chosen range of T_p, the examined sample exhibited dielectric (activation-like) behavior of the real part of admittance with $d\sigma/dT_p > 0$ [33]. This means that during carrier transport, electrons were forced to overcome dielectric barriers, tunneling between nanoparticles with conductance activation energies of $\Delta E_\sigma \approx (0.050 \pm 0.010)$ eV. Fig. 1b shows the frequency dependence of the phase shift angle θ, which has small negative values at $f < 10^3$ Hz (not more than 10° by modulo). This is typical capacitive behavior for composite granular samples. For the highest T_p values (>250 K), the θ values of the sample remain negative in the whole f range, although at low temperatures (<248 K) and high frequencies, the θ values become positive ('negative capacitance' effect in Fig. 1c), approaching +75°, which indicates the inductive-like behavior of the sample.

The transition from a positive capacitance to a negative capacitance is clearly shown in Fig. 1c, which presents the frequency dependence of the capacity modulo (C_p) measured in the parallel equivalent circuit regime. As shown in this figure, the C_p modulo quickly decreases with the increase of the frequency, reaching the expressed minimum for some frequency $f = f_{minC}$. After reaching the minimum value, the $C_p(f)$ modulo increases, eventually becoming saturated (steady state).

Comparison of Fig. 1b and 1c reveals that the frequencies at which minimal $C_p(f)$ modulo values are observed for every measurement temperature T_p coincide exactly with the f_θ values at which $\theta = 0$. The capacity modulo C_p in the frequency range $f < f_{minC}$ increased with the measurement temperature. Additionally, with the increase of the temperature, f_{minC} shifted to a region of higher frequencies. This resulted in an activational characteristic of the

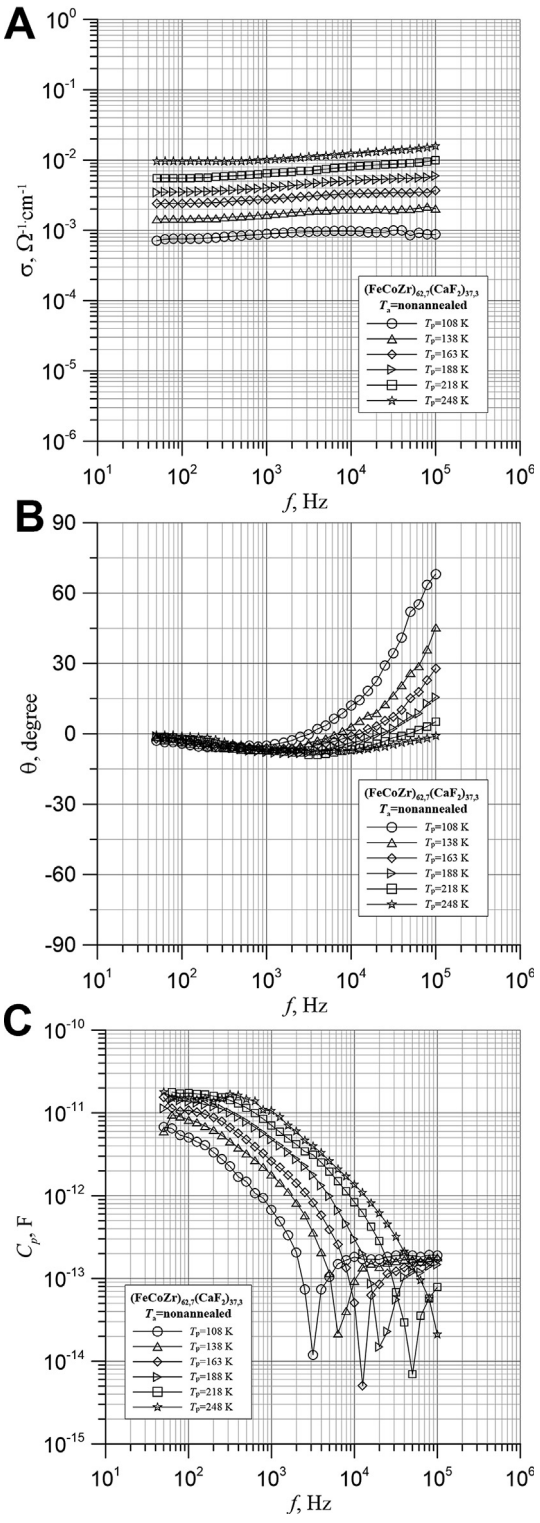

Fig. 1. Frequency dependences of the real part of the admittance σ (*a*), the phase shift angle θ (*b*), and the capacity modulo C_p (*c*) for the as-deposited $(FeCoZr)_{62.7}(CaF_2)_{37.3}$ nanocomposite sample in the temperature range of 81 K < T_p < 313 K.

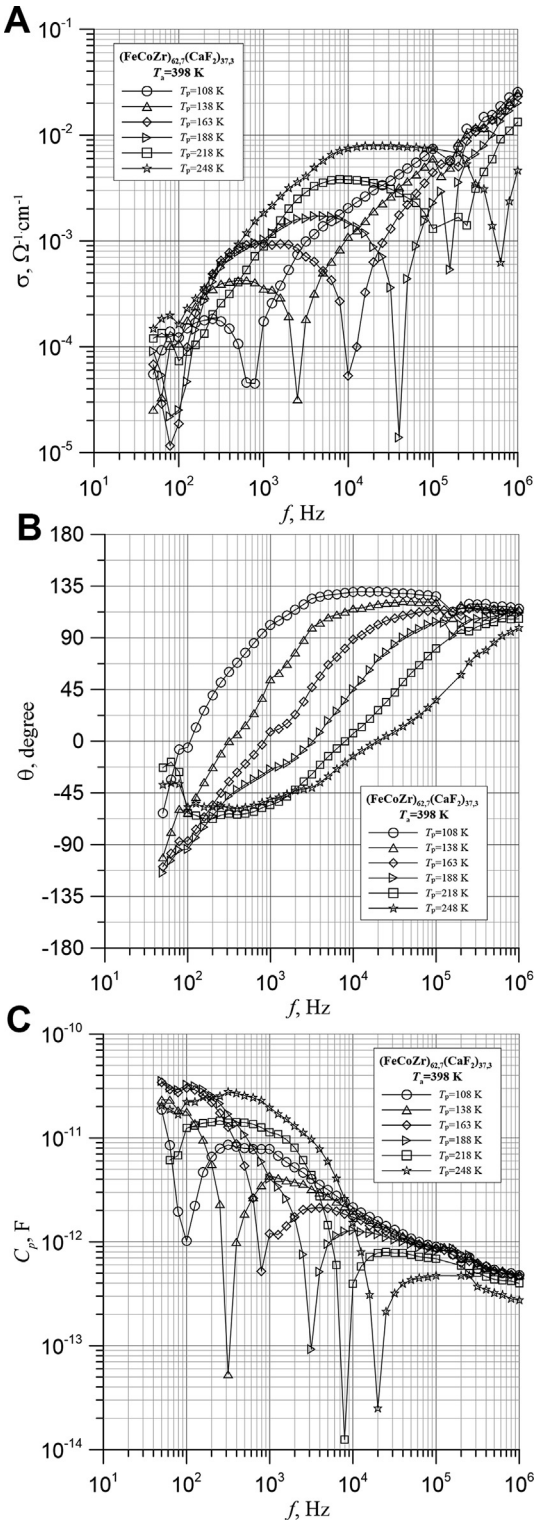

Fig. 2. Frequency dependences of the real part of the admittance σ (*a*), the phase shift angle θ (*b*), and the capacity modulo C_p (*c*) in the temperature range of 81 K < T_p < 313 K for the $(FeCoZr)_{62.7}(CaF_2)_{37.3}$ nanocomposite sample annealed at 398 K.

reactive part of the conductance. By plotting the $C_p(T_p)$ dependence on the Arrhenius scale, we observe that the thermal activation energy for this contribution $\Delta E_c \approx (0.041 \pm 0.010)$ eV is slightly lower than the aforementioned ΔE_σ values. As a whole, such behaviour of the $\sigma(f, T_p)$, $\theta(f, T_p)$, and $C_p(f, T_p)$ dependences of the studied nanocomposites is in accordance with the parallel equivalent *RCL* circuit where the contribution of *L* dominates over that of *C*.

As shown in Fig. 2, after 15 min of annealing at 398 K, the $\sigma(f, T_p)$,

θ(*f*, T_p), and C_p(*f*, T_p) dependences were significantly changed compared with those in Fig. 1, with regard to both their shape and turndown. The main differences in the σ(*f*, T_p), θ(*f*, T_p), and C_p(*f*, T_p) curves between the as-deposited and annealed samples are as follows. First, as shown in Fig. 2a, the σ(*f*) curves for the annealed samples exhibit a non-monotonous shape with two (or even three at some temperatures) minima whose positions on the frequency scale are strongly dependent on the temperature. Second, the θ(*f*) curves after the annealing process exhibit very strong widening of the θ values (from −120° to +135°) in the studied range of frequencies (Fig. 2b). Third, the C_p(*f*) progress with the increase of the frequency was conserved as a whole after the heat treatment, but the f_{minC} values were shifted to a lower range of frequencies with the decrease of the temperature (Fig. 2c). Fourth, the σ(*f*, T_p) curves in Fig. 2c show two minima that were absent for the as-deposited samples.

To explain the observed changes, let us analyse them in further detail with regard to the theory of admittance spectroscopy, considering the modes of measurement applied in the aforementioned *RCL*-meters. The joint analysis of the σ(*f*, T_p), θ(*f*, T_p), and C_p(*f*, T_p) curves transformed by heat treatment shows that the observed frequency dependences can be explained using equivalent circuits more complicated than those employed for the as-deposited samples. In particular, within the framework of the AC/DC hopping model considered in Refs. [11,18,19], which describes the effect of 'negative capacitance,' the equivalent circuits of the annealed nanocomposite samples should include both series and parallel *RCL* parts. In Ref. [18], we introduced equivalent circuits to describe the σ(*f*, T_p) dependences for $(CoFeZr)_x(Al_2O_3)_{(100-x)}$ and $(CoFeZr)_x(PZT)_{(100-x)}$ nanocomposite films. This follows from not only the presence of a minimum in the C_p(*f*) curves at some $f = f_{minC}$ (close to $f_{min\theta}$, where the θ(*f*) dependence changes sign from negative to positive) but also the appearance of two extra minima in the σ(*f*) curves (Fig. 2a) when the θ(*f*) dependences cross the lines of θ = -90° ($f_{min\sigma1}$) and θ = +90° ($f_{min\sigma2}$). Therefore, the σ(*f*) dependences show two resonance frequencies $f_{min\sigma1}$ and $f_{min\sigma2}$, at which the compensation of the voltages on the capacitive (*C*) and inductive (*L*) components of the *RCL* equivalent circuits is evidenced. These voltages are in opposite phases (−90° and +90°), and their values at the characteristic frequencies are coincident. The measured values of f_{minC} in Fig. 2c are between them: $f_{min\sigma1} < f_{minC} < f_{min\sigma2}$.

Because of the parity of the voltages on the inductive and capacitive components and their opposite phases (−90° and +90°), the *L* and C values cannot be estimated simultaneously. This follows from the formula for the voltage on the reactive part of the impedance in a series circuit:

$$U = i_0\left(\omega L_S - \frac{1}{\omega C_S}\right), \tag{1}$$

where i_0 is the applied current amplitude, C_S is the capacitance, L_S is the inductance, and $\omega = 2\pi f$ is the angular frequency.

Equation (1) indicates at every frequency f_σ, the measured capacity reaches a very small value (theoretically zero), in accordance with the following expression:

$$\omega_\sigma L - \frac{1}{\omega_\sigma C} = 0, \tag{2}$$

where $\omega_\sigma = 2\pi f_\sigma$.

The measurements presented in Fig. 2 were performed when the frequency changed with steps of 10 points per decade, and for this reason, we were unlikely to measure a value of precisely zero. The minima of the C_p(*f*) modulo dependences shown in Fig. 2c are clearly observed owing to the strong observed changes of C_p(*f*) (two or more orders of magnitude around f_{minC} values). It is evident from Fig. 2a that the AC conductivity did not show any peculiarities at the resonance frequency f_{minC}, which is in accordance with the voltage resonance theory.

It should be emphasized that such behavior of the admittance frequency dependences was observed in a wide temperature range of ~130−~225 K (see Fig. 2b). Using the equations

$$\tau_\theta = \frac{1}{2\pi f_\theta} \text{ and } \tau_C = \frac{1}{2\pi f_{minC}}, \tag{3}$$

we can estimate the characteristic times for the electron hopping processes. The temperature dependences of the estimated characteristic times τ_θ and τ_C are presented in Arrhenius plots in Fig. 3. As shown, both the time constants are in the same region of values; thus, we can assume that $\tau_\theta \approx \tau_C$ for every measurement temperature. Moreover, as indicated by curve 1 in Fig. 3, the $\tau_\theta(T)$ and $\tau_C(T)$ dependences in the Arrhenius scale ($\lg\tau - 1{,}000/T$) are described by curves with two linear segments having different slopes, which correspond to two different activation energies. In the low-temperature range (100−145 K), the activation energy is $\Delta E_{1c} \approx (0.012 \pm 0.002)$ eV, whereas at higher temperatures, it is $\Delta E_{2c} \approx (0.061 \pm 0.005)$ eV.

Similarly, we can compare the values of the characteristic times τ_{-90}, τ_{+90}, $\tau_{\sigma1}$, and $\tau_{\sigma2}$, which were estimated using the following equations:

$$\tau_{-90} = \frac{1}{2\pi f_{-90}} \qquad \tau_{90} = \frac{1}{2\pi f_{90}}$$
$$\tau_{\sigma1} = \frac{1}{2\pi f_{min\sigma1}} \qquad \tau_{\sigma2} = \frac{1}{2\pi f_{min\sigma2}} \tag{4}$$

They are also presented in Fig. 3. As shown, the time constants (τ_{-90}, $\tau_{\sigma1}$ and τ_{+90}, $\tau_{\sigma2}$) calculated from the temperature dependences of the phase angle shift for ($\theta = -90°$ and $f = f_{min\sigma1}$) and ($\theta = +90°$ and $f = f_{min\sigma2}$) are in coincidence in pairs (see curves 2 and 3). The appropriate activation energies are close to the values obtained above from the $\lg\tau_C(1{,}000/T)$ curves.

Let us analyse the observed frequency dependences of the AC

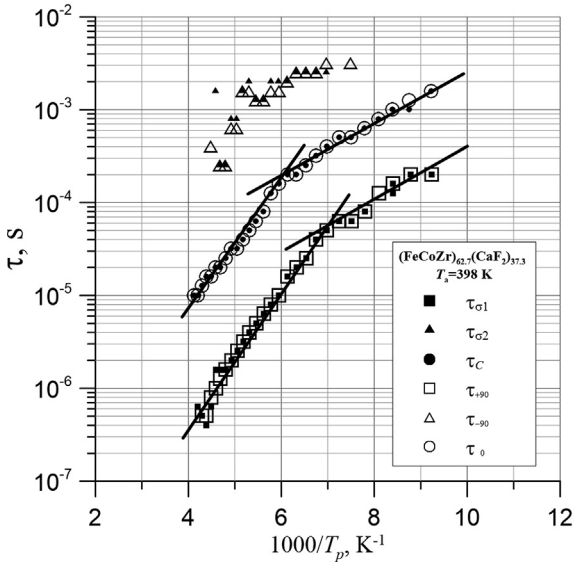

Fig. 3. Arrhenius plots for the characteristic time constants τ_C, τ_θ, $\tau_{\sigma1}$, $\tau_{\sigma2}$, τ_{-90}, and τ_{+90} (Equations (3) and (4)).

conductivity in further detail on the basis of conventional *RLC* circuits. The obvious minima in the $\sigma(f, T_p)$ curves indicate the presence of a current resonance in the two parallel circuits in the conventional equivalent *RLC* circuit. The resonance resistance R_R of these contributions is significantly higher than their active resistances r_P. The theory of current resonance shows that

$$R_R = \frac{L_P}{r_P C_P} \tag{5}$$

Hence,

$$\frac{R_R}{r_P} = \frac{L_P}{r_P^2 C_P} = Q^2 = \frac{1}{\tan^2 \delta}, \tag{6}$$

where Q is the quality factor and tanδ is the dielectric loss factor at the frequency where the current resonance occurs.

Fig. 4 shows the frequency dependence of tanδ(f), where both types of resonances (voltage and current) are clearly observed. For frequencies where the voltage resonance occurs, only the active component is observed, causing the tanδ values to increase to infinity. The impedance meters used in our experiments had a tanδ measurement limit of 10, as shown in Fig. 4. For the voltage resonance frequency (at $\theta = 0^\circ$), tanδ reached the maximal value of ~10 at every temperature. At approaching the frequencies, when $\theta = -90^\circ$ or $\theta = +90^\circ$, obvious minima of tanδ are observed with $\tan\delta \approx 3 \times 10^{-2} << 1$ (Fig. 4). This means (see Equation (6)) that the circuit resistance R_R at the current resonance frequency is approximately 1,000 times larger than the active resistance r_P of the circuit.

Analysis of Figs. 2–4 indicates that a complicated (series–parallel) equivalent circuit should be used to describe the AC hopping carrier transport in the annealed nanocomposite $(CoFeZr)_x(CaF_2)_{(100-x)}$ films. The occurrence of two minima in the $\sigma(f)$ dependences in the temperature range of 130–225 K indicates that the full equivalent circuit comprises two parallel circuits with two different systems of *RLC* parameters (see Fig. 5). The crossing of the zero line by the $\theta(f)$ dependences and the occurrence of obvious minima in the $C(f)$ curves at the same frequency ($f_\theta \approx f_{minC}$) indicate that the compound equivalent circuit of the nanocomposite film

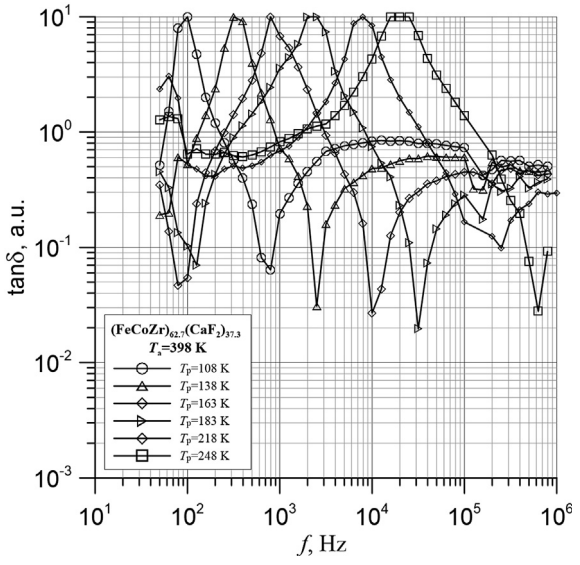

Fig. 4. Frequency dependences of the dielectric loss factor in the temperature range of 81 K < T_p < 313 K for the $(FeCoZr)_{62.7}(CaF_2)_{37.3}$ nanocomposite sample annealed at 398 K.

contains one series component in the equivalent circuit (Fig. 5). Current and voltage resonances occur in this *RLC* circuit at the angular frequency

$$\omega_R = \frac{1}{\sqrt{LC}} \tag{7}$$

For the series contribution to the equivalent circuit, the voltage resonance frequency is given as

$$\omega_{RS} = \frac{1}{\sqrt{L_S C_S}}, \tag{8}$$

and for two parallel parts of the equivalent circuit current, the resonance frequencies are equal to

$$\omega_{1RP} = \frac{1}{\sqrt{L_{1P} C_{1P}}} \text{ and } \omega_{2RP} = \frac{1}{\sqrt{L_{2P} C_{2P}}} \tag{9}$$

This indicates that the equivalent circuit of the annealed nanocomposite films presented in Fig. 5 contains three resistive components (R_S, R_{1P}, and R_{2P}), three capacitive components (C_S, C_{1P}, and C_{2P}), and three inductive components (L_S, L_{1P}, and L_{2P}), which can be attributed to the three-phase structure of the studied nanocomposite films (see the sketch in Fig. 5*b*).

Theoretical assumptions for the model of impedance and voltage resonance were described in the paper [34] and the modeling related to the occurrence of current resonance in the paper [18]. Resonance occurs in each electrical circuit for pulsations at which the resultant reactance of circuit X or the resultant susceptance B of the circuit is zero. A prerequisite for resonance is the simultaneous presence of reactance elements in the circuit: inductance and capacity. In the case of voltage resonance, there is compensation of induction reactance X_L with capacitance X_C and the total reactance is zero. At current resonance, the resulting susceptance of the circuit is zero. As proven in [18, 34], the presence of an inductive contribution in the equivalent circuit of nanocomposites with a 'core–shell' structure of FeCoZr-based nanoparticles is due to hopping (tunneling) of electrons between nanoparticles (neutral potential wells), which form electric dipoles. The electric dipoles cause the thermally activated polarization of the matrix around the nanoparticles, and the activation energy increases with the temperature. This results in the delay of the electron on the second nanoparticle after its first jump from the first nanoparticle under the weak AC bias voltage applied. Introduction of the characteristic time τ_σ of this delay of the electron on the second nanoparticle before its return to the first potential well or its jump to the third one (at the appropriated phase of the applied AC electric field or under phonons with appropriate energy) allows the high-frequency admittance to be described in accordance with the current resonance theory.

Examination of the annealed nanocomposite sample with close composition but deposited via ion-beam sputtering in a pure argon atmosphere at a partial pressure of $p_{Ar} = 1.1 \times 10^{-1}$ Pa proves that oxygen and fluorine had a significant impact on the occurrence of current resonance and the dominance of the inductive-like contribution over the capacitive one. Fig. 6 shows the frequency dependences of the phase angle θ for the $(FeCoZr)_{66.3}(CaF_2)_{33.7}$ nanocomposite sample (its composition is very similar to that described in Figs. 1 and 2), which was annealed under the same conditions. As shown, this sample is characterized by only capacitive-like behavior (no 'negative capacitance' or current resonances effects). In the context of the current resonance theory and the AC hopping model [11,18,19,34], we attribute the observed difference in the frequency dependences of the conductivity, capacity, phase angle, and dielectric loss factor of the annealed

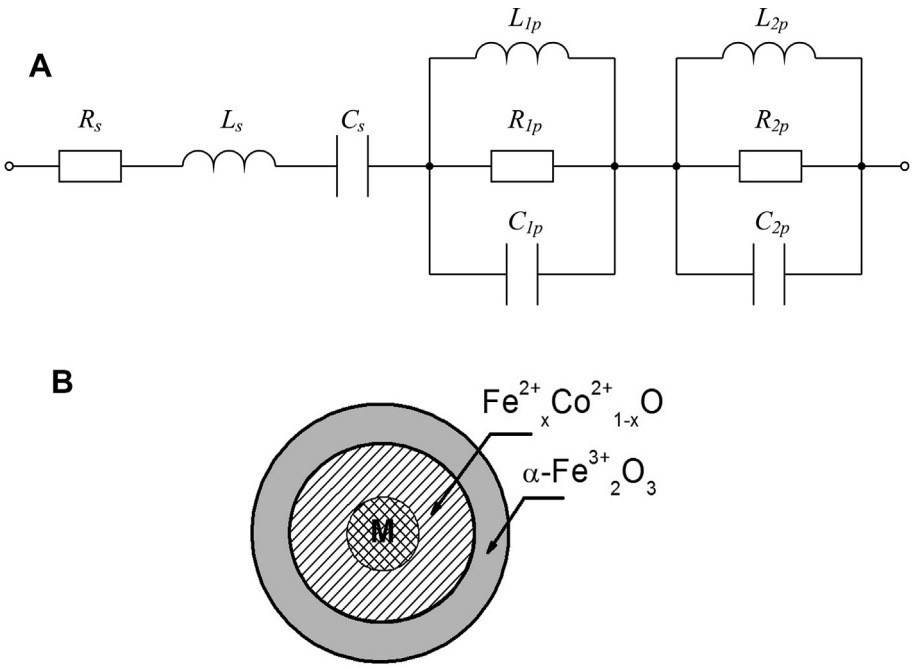

Fig. 5. Equivalent circuit for the $(FeCoZr)_{62.7}(CaF_2)_{37.3}$ nanocomposite annealed at 398 K (*a*) and a sketch of the 'core−shell' nanoparticle composition (*b*), where M denotes the α-FeCo(Zr) 'core'.

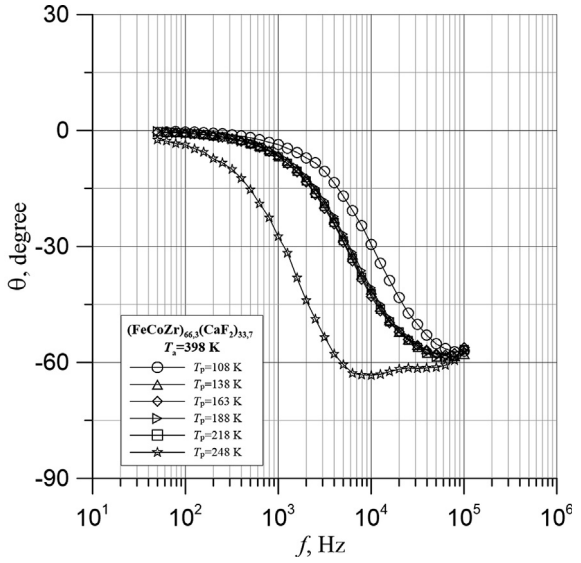

Fig. 6. Frequency dependences of the phase shift angle θ in the temperature range of 81 K < T_p < 313 K for the $(FeCoZr)_{66.3}(CaF_2)_{33.7}$ nanocomposite sample annealed at 398 K.

samples $(FeCoZr)_{62.7}(CaF_2)_{37.3}$ and $(FeCoZr)_{66.3}(CaF_2)_{33.7}$ to the different phase compositions of the nanoparticles due to the involvement of not only oxygen but also fluorine atoms in the formation of 'shells' at the surface of the metallic nanoparticles.

Next, we discuss possible reasons for the different behavior of both the $(Fe_{45}Co_{45}Zr_{10})_x(CaF_2)_{(100-x)}$ annealed films from the previously studied annealed $(Fe_{45}Co_{45}Zr_{10})_x(Al_2O_3)_{100-x}$ or $(Fe_{45}Co_{45}Zr_{10})_x(Pb(ZrTi)O_3)_{(100-x)}$ nanogranular films, as well as the differences between the frequency dependences of the admittance for the $(FeCoZr)_{62.7}(CaF_2)_{37.3}$ and $(FeCoZr)_{66.3}(CaF_2)_{33.7}$ films in the temperature range of 81 K < T_p < 313 K, as shown in Figs. 2 and 6.

A detailed study of as-deposited $(FeCoZr)_{62.7}(CaF_2)_{37.3}$ and $(FeCoZr)_{66.3}(CaF_2)_{33.7}$ films using XRD and Mössbauer spectroscopy [35] revealed that 'core−shell' nanoparticles contain three phases: metallic 'cores' (phase *I*) and two types of FeCo-based oxides in 'shells' (see Fig. 5b). The first oxide (phase *II*) is a crystalline $Fe^{2+}_yCo^{2+}_{1-y}O$ phase, and the second oxide (phase *III*) is α-Fe_2O_3 with a high degree of structural disorder. According to the data reported in Refs. [25,34], where the process of nanoparticle oxidation was considered in detail, we believe that the crystalline $Fe^{2+}_xCo^{2+}_{1-x}O$ phase is localized between the α-FeCo(Zr) 'core' surface and the α-Fe_2O_3 disordered oxide. The α-Fe_2O_3 oxide is formed mainly at the interface with the CaF_2 matrix; thus, the structural disorder and dissolution of F atoms in this oxide may be due to its location near fluorite. In addition to structure and crystallinity, these oxides differ with regard to their magnetic and electrical properties [25].

The main difference between the phase compositions of the $(FeCoZr)_{62.7}(CaF_2)_{37.3}$ (sample production in argon with the addition of oxygen) and $(FeCoZr)_{66.3}(CaF_2)_{33.7}$ (sample produced in pure argon) films is the ratio of metallic-to-oxide contributions. Progressive oxidation occurs with the increase of *x* [35]; thus, almost complete Fe oxidation occurs in the $(FeCoZr)_{66.3}(CaF_2)_{33.7}$ sample, whereas the metallic core contains mainly Co (as shown in Fig. 5b). Based on the analysis of Mössbauer spectroscopy spectra, it was calculated that about 20% of Fe and Co elements are in the metallic phase [36]. The remaining atoms of these elements are in the form of oxides. Less than 20 at.% of Fe is in the metallic (non-oxidized) state in this sample (according to Mössbauer spectroscopy). The contribution of $Fe^{2+}_xCo^{2+}_{1-x}O$ oxide also dramatically increases. Thus, the main phase transformations in the nanoparticles with the increase of $x \geq 62.7$ at.% are related to the decrease of the metallic 'core'-to-$Fe^{2+}_yCo^{2+}_{1-y}O$ oxide ratio and, as a result, the increase of the $Fe^{2+}_yCo^{2+}_{1-y}O$ oxide-to-α-Fe_2O_3 ratio (because of the redistribution in the oxide shell).

Similar frequency dependences of the conductance, capacitance phase angle, and dielectric loss factor for the $(Fe_{45}Co_{45}Zr_{10})_x(CaF_2)_{(100-x)}$ annealed films were observed at high annealing temperatures (423 K ≤ T_a ≤ 573 K). However, the impact of the high-temperature annealing on the recorded dependences was

considerably smaller than that of annealing at 398 K (low temperature). This may be related to the high chemical activity of oxygen and especially fluorine ions. After the first (low-temperature) annealing at 398 K, almost all the free ions of fluorine and oxygen, defragmented by the film during the deposition procedure, fully reacted chemically with the metallic atoms incorporating into phases *II* and *III*. Further annealing at higher temperatures caused significantly slower structural changes of the nanocomposite owing to the deficiency of free F and O atoms for the samples, especially with high *x* values.

It is still unknown which of these three phases (along with three time constants and three systems of *RLC* parameters) are related to the voltage resonance or the current resonances. This question requires additional experiments.

4. Conclusions

Low-temperature annealing (at 398 K) of $(FeCoZr)_x(CaF_2)_{(100-x)}$ nanocomposite films produced with ion-beam sputtering in an argon−oxygen gas mixture caused significant changes of the AC electrical properties. The θ changes for a $(FeCoZr)_{62.7}(CaF_2)_{37.3}$ film sample after annealing at 398 K were measured within the range of −170° to +135°, exceeding the characteristic limit of $\theta = \pm 90°$ for conventional *RLC* circuits. A clear minimum was observed in the $C(f, T_p)$ modulo dependences when the phase angle θ approached zero. The presence of this minimum is similar to the phenomenon of voltage resonance in series *RLC* circuits. Additionally, the dependences of $\sigma(f)$ exhibited two obvious minima related to the transition of the phase shift angle through the values $\theta_1 = +90°$ and $\theta_2 = -90°$. Such behavior corresponds to the current resonances in conventional parallel *RLC* circuits. The AC parameters of the $(FeCoZr)_x(CaF_2)_{(100-x)}$ films annealed at temperatures of $T_a \approx 398$ K were described by using a compound equivalent circuit comprising one series *RLC* circuit and two parallel circuits, which differed in the values of their *R*, *L*, and *C* elements. In our opinion, this is related to the formation of the three-phase structure of the nanocomposite films, which involved the electron hopping process under the applied AC bias voltage. These phases are metallic 'cores' (phase *I*) and two types of FeCo-based oxides 'shells' ($Fe_x^{2+}Co_{1-x}^{2+}O$ crystalline oxide, i.e., phase *II*, and α-Fe_2O_3 disordered oxide, i.e., phase *III*) between the metallic core and the CaF_2 matrix.

Joint analysis of the $\sigma(f)$, $\theta(f)$, $C_p(f)$, and $\tan\delta(f)$ curves transformed by heat treatment revealed that the observed frequency dependences can be explained by the previously developed AC/DC hopping model with three different characteristic times of electron hopping and three sets of parameters for the three components of the full equivalent circuit in Fig. 5 (R_S, C_S, L_S; R_{1P}, C_{1P}, L_{1P}; R_{2P}, C_{2P}, L_{2P}) owing to the different tunneling conditions between the aforementioned three-phase nanoparticles embedded in the transparent ceramic matrix. It is still unknown which of these time constants and *RLC* parameters are related to the voltage resonance or current resonances.

Considering such nanocomposite $(FeCoZr)_x(CaF_2)_{(100-x)}$ properties and using ion beam sputtering technologies, one can obtain an area without winding inductance with about 100 μH/μm^3 induction and capacity with relative dielectric permittivity of about 10,000 in one technological process. Consequently, it allows reducing the surface area of the semiconductor structure while increasing the degree of integration and the use of such materials in integrated circuits.

Author contributions section

T.N. Kołtunowicz − Conceptualization; Investigation; Participation in writing - original draft; Project administration; Participation in writing − review & editing; Funding acquisition.

V. Bondariev − Investigation; Data curation; Visualization; Funding acquisition.

P. Żukowski − Formal analysis; Methodology; Supervision; Funding acquisition.

J.A. Fedotova − Data curation; Formal analysis; Methodology.

A.K. Fedotov − Conceptualization; Methodology; Participation in writing - original draft; Participation in writing − review & editing; Funding acquisition.

Declaration of competing interest

The authors declare that they have no conflict of interest.

Acknowledgements

The Minsk group thanks The State Programme of Belarus 'Functional and composite materials, nanomaterials' (project 1.37) for the partial financial support of this research.

This research was partially supported by the Polish Ministry of Science and Higher Education as a science fund of the Lublin University of Technology, at the Faculty of Electrical Engineering and Computer Science, FN-28/E/EE/2019 − *Researches of electrical, magnetic, thermal and mechanical properties of modern electrotechnical and electronic materials, including nanomaterials and diagnostic of electrical devices and their components*.

References

[1] S.K. Mishra, S.N. Tripathi, V. Choudhary, B.D. Gupta, SPR based fibre optic ammonia gas sensor utilizing nanocomposite film of PMMA/reduced graphene oxide prepared by in situ polymerization, Sens. Actuators B Chem. 199 (2014) 190−200.

[2] G. Zhou, X. Tan, Y. Pei, K. Fan, M. Qiao, B. Sun, B. Zong, Structural and catalytic properties of alkaline post-treated Ru/ZrO_2 catalysts for partial hydrogenation of benzene to cyclohexene, ChemCatChem 5 (2013) 2425−2435.

[3] T.L. Wang, C.H. Yang, Y.T. Shieh, A.C. Yeh, Synthesis of CdSe-Poly(*N*-vinylcarbazole) nanocomposite by atom transfer radical polymerization for potential optoelectronic applications, Macromol. Rapid Commun. 30 (2009) 1679−1683.

[4] A. Fathy, O. Elkady, A. Abu-Oqail, Microstructure, mechanical and wear properties of $Cu-ZrO_2$ nanocomposites, Mater. Sci. Technol. 33 (2017) 2138−2146.

[5] A.D. Pogrebnjak, V.M. Beresnev, Nanocoatings Nanosystems Nanotechnologies, Bentham Books, 2012.

[6] YaO. Kravchenko, L.E. Coy, B. Peplinska, I. Iatsunskyi, K. Zaleski, M. Kempinski, V.M. Beresnev, P. Konarski, S. Jurga, A.D. Pogrebnjak, Nano-multilayered coatings of (TiAlSiY)N/MeN (Me=Mo, Cr and Zr): influence of composition of the alternating layer on their structural and mechanical properties, J. Alloy. Comp. 767 (2018) 483−495.

[7] J.V. Kasiuk, J.A. Fedotova, M. Marszalek, A. Karczmarska, M. Mitura-Nowak, Y.E. Kalinin, A.V. Sitnikov, Effect of oxygen pressure on phase composition and magnetic structure of FeCoZr-Pb(ZrTi)O_3 nanocomposites, Phys. Solid State 54 (2012) 178−184.

[8] M. Lu, M. Liu, L. Wang, S. Xu, J. Zhao, H. Li, Structural and magnetic properties of $CoFe_2O_4/CoFe_2/SiO_2$ nanocomposites with exchange coupling behavior, J. Alloy. Comp. 690 (2017) 27−30.

[9] T.N. Kołtunowicz, P. Zukowski, J. Sidorenko, V. Bayev, J.A. Fedotova, M. Opielak, A. Marczuk, Ferromagnetic resonance spectroscopy of CoFeZr-Al_2O_3 granular films containing "FeCo core − oxide shell" nanoparticles, J. Magn. Magn. Mater. 421 (2017) 98−102.

[10] R.S. Iskhakov, E.A. Denisova, S.V. Komogortsev, L.A. Chekanova, Y.E. Kalinin, A.V. Sitnikov, Ferromagnetic resonance and magnetic microstructure in nanocomposite films of $Co_x(SiO_2)_{1-x}$ and $(CoFeB)_x(SiO_2)_{1-x}$, Phys. Solid State 52 (2010) 2263−2266.

[11] T.N. Koltunowicz, P. Zukowski, M. Milosavljević, A.M. Saad, J.V. Kasiuk, J.A. Fedotova, Y.E. Kalinin, A.V. Sitnikov, A.K. Fedotov, AC/DC conductance in granular nanocomposite films $(Fe_{45}Co_{45}Zr_{10})_x(CaF_2)_{100-x}$, J. Alloy. Comp. 586 (2014) S353−S356.

[12] V. Demchenko, V. Shtompel, S. Riabov, Nanocomposites based on interpolyelectrolyte complex and Cu/Cu_2O core−shell nanoparticles: structure, thermomechanical and electric properties, Eur. Polym. J. 75 (2016) 310−316.

[13] T.N. Koltunowicz, P. Zukowski, K. Czarnacka, V. Bondariev, O. Boiko, I.A. Svito, A.K. Fedotov, Dielectric properties of nanocomposite $(Cu)_x(SiO_2)_{(100-x)}$ produced by ion-beam sputtering, J. Alloy. Comp. 652 (2015) 444−449.

[14] T.N. Koltunowicz, P. Zukowski, O. Boiko, K. Czarnacka, V. Bondariev, A. Saad,

A.V. Larkin, A.K. Fedotov, Capacitive properties of nanocomposite $(FeCoZr)_x(PZT)_{(100-x)}$ produced by sputtering with the use of argon and oxygen ions beam, J. Mater. Sci. Mater. Electron. 27 (2016) 1171–1176.
[15] I.A. Svito, A.K. Fedotov, A. Saad, P. Zukowski, T.N. Koltunowicz, Influence of oxide matrix on electron transport in $(FeCoZr)_x(Al_2O_3)_{1-x}$ nanocomposite films, J. Alloy. Comp. 699 (2017) 818–823.
[16] A.M. Saad, A.K. Fedotov, J.A. Fedotova, I.A. Svito, B.V. Andrievsky, Y.E. Kalinin, V.V. Fedotova, V. Malyutina-Bronskaya, A.A. Patryn, A.V. Mazanik, A.V. Sitnikov, Characterization of $(Co_{0.45}Fe_{0.45}Zr_{0.10})_x(Al_2O_3)_{1-x}$ nanocomposite films applicable as spintronic materials, Phys. Status Solidi C 3 (2006) 1283–1290.
[17] P. Zhukowski, T.N. Kołtunowicz, P. Węgierek, J.A. Fedotova, A.K. Fedotov, A.V. Larkin, Formation of Noncoil-Like Inductance in Nanocomposites $(Fe_{0.45}Co_{0.45}Zr_{0.10})_x(Al_2O_3)_{1-x}$ manufactured by ion-beam sputtering of complex targets in $Ar+O_2$ atmosphere, Acta Phys. Pol. A 120 (2011) 43–45.
[18] T.N. Kołtunowicz, J.A. Fedotova, P. Zhukowski, A. Saad, A. Fedotov, J. V Kasiuk, A.V. Larkin, Negative capacitance in (FeCoZr)-(PZT) nanocomposite films, J. Phys. D Appl. Phys. 46 (2013), 125304.
[19] T.N. Kołtunowicz, P. Zhukowski, V.V. Fedotova, A.M. Saad, A.K. Fedotov, Hopping Conductance in Nanocomposites $(Fe_{0.45}Co_{0.45}Zr_{0.10})_x(Al_2O_3)_{1-x}$ manufactured by ion-beam sputtering of complex target in $Ar+O_2$ ambient gas, Acta Phys. Pol. A 120 (2011) 39–42.
[20] H.L. Kwok, Modeling negative capacitance effect in organic polymers, Solid State Electron. 47 (2003) 1089–1093.
[21] A. Rusu, A. Saeidi, A.M. Ionescu, Condition for the negative capacitance effect in metal-ferroelectric-insulator-semiconductor devices, Nanotechnology 27 (11) (2016). Article Number: 115201.
[22] L. Bakueva, G. Konstantatos, S. Musikhin, H.E. Ruda, A. Shik, Negative capacitance in polymer-nanocrystal composites, Appl. Phys. Lett. 85 (2004) 3567–3569.
[23] J. Kyungmin, U. Nozomu, K. Masaharu, H. Toshiro, Experimental observation and simulation model for transient characteristics of negative-capacitance in ferroelectric $HfZrO_2$ capacitor, IEEE J. Electron Devices Soc. 6 (1) (2018) 346–353.
[24] J.A. Fedotova, J. Przewoznik, C. Kapusta, M. Milosavljević, J. V Kasiuk, J. Zukrowski, M. Sikora, A.A. Maximenko, D. Szepietowska, K.P. Homewood, Magnetoresistance in FeCoZr-Al_2O_3 nanocomposite films containing "metal core–oxide shell" nanogranules, J. Phys. D Appl. Phys. 44 (2011), 495001.
[25] J. Fedotova, J. Kasiuk, J. Przewoznik, C. Kapusta, I. Svito, Y. Kalinin, A. Sitnikov, Effect of oxide shells on the magnetic and magnetotransport characteristics of oxidized FeCoZr nanogranules in Al_2O_3, J. Alloy. Comp. 509 (2011) 9869–9875.
[26] O. Boiko, T.N. Koltunowicz, P. Zukowski, A.K. Fedotov, A.V. Larkin, The effect ofsputtering atmosphere parameters on dielectric properties of the ferromagnetic alloy – ferroelectric ceramics nanocomposite $(FeCoZr)_x(PbZrTiO_3)_{(100-x)}$, Ceram. Int. 43 (2017) 2511–2516.
[27] S.A. Gridnev, YuE. Kalinin, A.V. Sitnikov, O.V. Stognei, Nonlinear Phenomena in Nano- and Micro-heterogeneous Systems, BINOM, Labor. Znanii, Moscow, 2012 [in Russian].
[28] V.V. Rylkov, S.N. Nikolaev, V.A. Demin, A.V. Emelyanov, A.V. Sitnikov, K.E. Nikiruy, V.A. Levanov, M.Yu Presnyakov, A.N. Taldenkov, A.L. Vasiliev, K.Yu Chernoglazov, A.S. Vedeneev, YuE. Kalinin, A.B. Granovsky, V.V. Tugushev, A.S. Bugaev, Transport, magnetic, and memristive properties of a nanogranular $(CoFeB)_x(LiNbO_y)_{100-x}$ composite material, J. Exp. Theor. Phys. 126 (3) (2018) 353–367.
[29] F.F. Komarov, P. Zukowski, R.M. Kryvasheyeu, E. Munoz, T.N. Koltunowicz, V.N. Rodionova, A.K. Togambaeva, Effects of surfactant and fabrication procedure on the electrical conductivity and electromagnetic shielding of single-walled carbon nanotube films, Status Solidi A Appl. Mater. 212 (2015) 425–432.
[30] T.N. Koltunowicz, Test station for frequency-domain dielectric spectroscopy of nanocomposites and semiconductors, J. Appl. Spectrosc. 82 (2015) 653–658.
[31] T.N. Koltunowicz, P. Zukowski, V. Bondariev, A.K. Fedotov, I. Svito, J. Fedotova, A. Saad, Voltage and current resonance in nanocomposite $(FeCoZr)_x(CaF_2)_{100-x}$ produced by ion-beam sputtering in pure argon atmosphere, Acta Phys. Pol. 128 (2015) 897–901.
[32] T.N. Koltunowicz, P. Zukowski, V. Bondariev, J.A. Fedotova, A.K. Fedotov, The effect of annealing on induction like properties of $(FeCoZr)_x(CaF_2)_{(100-x)}$ nanocomposite films produced by ion-beam sputtering in the vacuum environment, Vacuum 120 (2015) 44–50.
[33] Y. Imry, Introduction to Mesoscopic Physics, Oxford University Press, 2002.
[34] T.N. Kołtunowicz, P. Żukowski, O. Boiko, V. Bondariev, K. Czarnacka, J.A. Fedotova, A.K. Fedotov, I.A. Svito, Impedance model of metal-dielectric nanocomposites produced by ion-beam sputtering in vacuum and its experimental verification for thin films of $(FeCoZr)_x(PZT)_{(100-x)}$, Vacuum 120 (2015) 37–43. Part B.
[35] J.V. Kasiuk, J.A. Fedotova, T.N. Koltunowicz, P. Zukowski, A.M. Saad, J. Przewoznik, C. Kapusta, J. Zukrowski, I.A. Svito, Correlation between local Fe states and magnetoresistivity in granular films containing FeCoZr nanoparticles embedded into oxygen-free dielectric matrix, J. Alloy. Comp. 586 (2014) S432–S435.
[36] J. Kasiuk, J. Fedotova, J. Przewoźnik, C. Kapusta, M. Sikora, J. Żukrowski, A. Grce, M. Milosavljević, Oxidation controlled phase composition of FeCo(Zr) nanoparticles in CaF_2 matrix, Mater. Char. 113 (2016) 71–81.